II International Conference on Particle-based Methods – Fundamentals and Applications
Particles 2011
E. Oñate and D.R.J. Owen (Eds)

A GENERAL COMPARETIVE STUDY IN LONG ROD PENETRATION USING CORRECTIVE SMOOTHED PARTICLE METHOD

A. EGHTESAD [*], A. R. SHAFIEI [†]

[*] Yazd University
Mechanical engineering department, Iran
e-mail: a.eghtesad@stu.yazduni.ac.ir

[†] Yazd University
Mechanical engineering department, Iran
e-mail: arshafiei@yazduni.ac.ir

Keywords: CSPM, Long Rod Penetration, Impact, FGM.

Abstract. Corrective smoothed particle method (CSPM) has been used to study the dynamic behavior of targets with different materials; AL, ALN and AL-ALN FGM in long rod penetration of an AL projectile. A mixed strength model with sigmoid formulation has been used to describe both yielding and fracture phenomena in the FGM. The strength model includes the JC dynamic yield relation and JHB fracture model with a continuum damage description approach. An efficient renormalization in continuity density approach is used to improve the SPH approximation of boundary physical variables. This study shows that the CSPM method in combination with the proper strength model describing the FGM dynamic behavior, can predict the mixed plastic and brittle response of different materials in long rod penetration problems.

1 INTRODUCTION

FGMs, as a new generation of materials, are widely used in heat barrier systems, aerospace industries and energy absorbing applications. In armor systems, there hase been an attempt to predict the dynamic behavior of FGMs under high velocity impact conditions. Recent researches confirm the importance of study of FGMs in the field of dynamic response of materials.

Smoothed particle hydrodynamics (SPH) is a particle and meshless method that has promising advantages in modeling problems with extreme large deformations that include brittle damage and fracture in ceramics. SPH was first proposed to solve cosmological problems in three-dimensional open space such as the simulations of binary stars and stellar collisions [1, 2]. The SPH method has also been applied extensively in computational fluid dynamics related areas that include multi-phase flows [3], incompressible flow simulations [4, 5], free surface flow analysis [6, 7].

In this paper, Corrective smoothed particle method (CSPM) has been used to study the dynamic behavior of targets with different materials; AL, ALN and AL-ALN FGM in long rod penetration problem. A mixed Strength model with sigmoid formulation has been used to

describe both yielding and fracture phenomena in the FGM. Temperature field is evaluated from a heat conduction equation with variable thermal conductivity and the result is used in Johnson-Cook yield model. The presented paper shows that using a functionally graded which macroscopic behavior is described using a sigmoid function, will be resistant enough to penetration of high velocity projectiles. The CSPM method in combination with the proper strength model describing the FGM dynamic behavior, can predict the mixed plastic and brittle response of a ceramic–metal functionally graded material in high velocity impact phenomena and the related fields.

2 SMOOTHED PARTICLE HYDRODYNAMICS

In a SPH formulation, every arbitrary function, $f(x)$ and its derivative can be expressed using the equations 1, 2, respectively.

$$f_i(r) = \sum_j \frac{m_j}{\rho_j} f_j W\left(r - r_j, h\right), \tag{1}$$

$$\nabla f_i(r) = \sum_j \frac{m_j}{\rho_j} f_j \nabla W\left(r - r_j, h\right), \tag{2}$$

Where in above equations, m_j, ρ_j are the mass and density of neighbor particle j, and $W(r - r_j, h)$ is the kernel function that is covering the support domain with a radius of $2h$.

2.1 Continuity equation

The continuity equation in a SPH algorithm can be written as follows:

$$\frac{D\rho_i}{Dt} = \rho_i \sum_j \frac{m_j}{\rho_j}\left(v_i - v_j\right).\nabla W\left(r - r_j, h\right), \tag{3}$$

Where, $v_i - v_j$ is the relative velocity between particles i, j.

2.2 Momentum equation

In the absence of the body force, the momentum equation which is commonly used in SPH applications has the following form:

$$\frac{Dv_i}{Dt} = \sum_j m_j \left(\frac{\sigma_i^{\alpha\beta}}{\rho_i^2} + \frac{\sigma_j^{\alpha\beta}}{\rho_j^2} + \Pi_{ij} \right) \frac{\partial W\left(r - r_j, h\right)}{\partial x_i^{\beta}}, \tag{4}$$

Where, $\sigma_i^{\alpha\beta}$ is the total stress tensor with the following relation:

$$\sigma^{\alpha\beta} = -P\delta^{\alpha\beta} + S^{\alpha\beta}. \tag{5}$$

In the above equation, P, is the hydrodynamic pressure, $\delta^{\alpha\beta}$, is the component of identity tensor, and $S^{\alpha\beta}$ is the component of deviatoric part of stress tensor. The rate of change of deviatoric stress tensor due to time can be expressed as follows:

$$\frac{Ds^{\alpha\beta}}{Dt} = 2G\left(\dot{\varepsilon}^{\alpha\beta} - \frac{1}{3}\delta^{\alpha\beta}\dot{\varepsilon}^{\gamma\gamma}\right) + S^{\alpha\gamma}\Omega^{\gamma\beta} + \Omega^{\alpha\gamma}S^{\gamma\beta}, \tag{6}$$

Where, $\dot{\varepsilon}^{\alpha\beta}$, is the component of strain rate tensor and is given by:

$$\dot{\varepsilon}^{\alpha\beta} = \frac{1}{2}\sum_j \frac{m_j}{\rho_j}\left\{\left(v_j{}^{\alpha} - v_i{}^{\alpha}\right)\frac{\partial W\left(r-r_j\ ,h\right)}{\partial x_i{}^{\beta}} + \left(v_j{}^{\beta} - v_i{}^{\beta}\right)\frac{\partial W\left(r-r_j\ ,h\right)}{\partial x_i{}^{\alpha}}\right\}. \tag{7}$$

In a same manner, for $\Omega^{\alpha\beta}$, the component of rotation rate tensor, we have:

$$\Omega^{\alpha\beta} = \frac{1}{2}\sum_j \frac{m_j}{\rho_j}\left\{\left(v_j{}^{\alpha} - v_i{}^{\alpha}\right)\frac{\partial W\left(r-r_j\ ,h\right)}{\partial x_i{}^{\beta}} - \left(v_j{}^{\beta} - v_i{}^{\beta}\right)\frac{\partial W\left(r-r_j\ ,h\right)}{\partial x_i{}^{\alpha}}\right\} \tag{8}$$

In equation (4), the term Π_{ij} is artificial viscosity.

3 CSPM CORRECTION ALGORITHM

To reduce the errors in free surface boundaries, a renormalization scheme have been used which is called corrective smoothed particle method (CSPM). CSPM scheme is first proposed by Chen in [8] and specifically is used to normalize the density continuity approach in a SPH algorithm. The CSPM correction can be defined as follows:

$$\frac{D\rho_i}{Dt} = \frac{\rho_i \sum_j \frac{m_j}{\rho_j}\left(v_i - v_j\right).\nabla W(r-r_j\ ,h)}{\sum_j \frac{m_j}{\rho_j}\left(r_i - r_j\right).\nabla W(r-r_j\ ,h)} \tag{9}$$

4 EQUATION OF STATE (EOS)

4.1 Tillotson EOS

The Tillotson EOS was suggested by Tillotson in 1962 [9] for describing the dynamic behavior of metals in high pressures and high rates of plastic strain including phase transition. In this form of EOS, the Hugoniot pressure–volume space is considered to be four distinct regions with the following pressure-density relations in different zones of material:

5 DYNAMIC YIELD MODEL

5.1 Johnson-Cook dynamic yield model

The Johnson-Cook dynamic yield model can be expressed as [10]:

$$\sigma = \left[A + B\varepsilon^n\right]\left[1 + Cln\dot{\varepsilon}^*\right]\left[1 - T^{*m}\right], \tag{10}$$

Where:

$$T^* = \frac{T - T_{ambient}}{T_{Melt} - T_{ambient}}, \tag{11}$$

$$\dot{\varepsilon}^* = \frac{\dot{\varepsilon}}{\dot{\varepsilon}_0}.$$

ε, $\dot{\varepsilon}^*$, $\dot{\varepsilon}$, $\dot{\varepsilon}_0$ T, $T_{ambient}$, T_{melt} are the equivalent plastic strain, dimensionless equivalent strain rate, equivalent plastic strain rate, reference equivalent plastic strain rate, ambient temperature and melting temperature, respectively.

6 FAILURE MODEL

6.1 JHB failure model

JHB [11] is a new modification of JH1 and JH2, the two previous failure models offered by Johnson and Holmquist [12, 13]. The advantage of JHB failure model is including a phase change from solid to gas during failure process.
JHB strength model can be written as follows:
For intact material:

$$\sigma = \{\sigma_i + (\sigma_{max} - \sigma_i)\{1 - \exp[-\alpha_i (P - P_i)]\}\}\left(1 + C_{JHB} ln\, \dot{\varepsilon}^*\right), \tag{12}$$

Where:

$$\alpha_i = \frac{\sigma_i}{[(\sigma_{max} - \sigma_i)(P_i + T)]}, \qquad \dot{\varepsilon}^* = \frac{\dot{\varepsilon}}{\dot{\varepsilon}_0}. \tag{13}$$

In above equations, σ_i is the intact stress, σ_{max} is the maximum strength, P_i is the intact pressure, C_{JHB} is a constant between 0 and 1, $\dot{\varepsilon}$ is the equivalent plastic strain rate, $\dot{\varepsilon}^*$ is the dimensionless equivalent strain rate.
For failed material:

$$\sigma = \{\sigma^f{}_{max} + (\sigma_{max} - \sigma_f)\{1 - \exp[-\alpha_f (P - P_f)]\}\}\left(1 + C_{JHB} ln\, \dot{\varepsilon}^*\right), \tag{14}$$

Where:

$$\alpha_f = \frac{\sigma_f}{[P_f (\sigma^f{}_{max} - \sigma_f)]}. \tag{15}$$

7 FGM MIXED PROPERTIES

One of the best methods for defining the macroscopic behavior of a FGM is called sigmoid function [14]. As Chung and Chi have pointed out in [15], the sigmoid function can reduce the stress intensity significantly in the ceramic-metal transition band. The sigmoid function for a plate with thickness of h can be written as:

$$X(z)=\begin{cases} g_1(z)X_1+\left[1-g_1(z)X_2\right], & 0\le z\le h/2 \\ g_2(z)X_1+\left[1-g_2(z)X_2\right], & -h/2\le z\le 0 \end{cases}, \tag{16}$$

Where, $X(z)$ is an arbitrary physical property of the FGM (e.g. density, modulus of elasticity, shear modulus). The functions, $g_1(z)$, $g_2(z)$, can be expressed using the following relations:

$$g_1(z)=1-\frac{1}{2}\left(\frac{\frac{h}{2}-z}{\frac{h}{2}}\right)^p \quad \text{For } 0\le z\le \frac{h}{2}, \tag{17}$$

$$g_2(z)=\frac{1}{2}\left(\frac{\frac{h}{2}+z}{\frac{h}{2}}\right)^p \quad \text{For } -h/2\le z\le 0. \tag{18}$$

Where, P, is a constant parameter depending on the fabrication process of the FGM. Figure 1 shows the variation of an arbitrary physical property, X, for different values of P, in a sigmoid FGM plate [14].

8 DEFINING THE FGM MIXED STRENGTH MODEL

The most important issue in modeling of a FGM to be as target in an impact problem, is finding a suitable combination of the dynamic yield model for pure metal and failure model for ceramic. In a FGM band, the material is not pure ductile like metal nor brittle like ceramic but is somewhat between them, so, we used the sigmoid function for defining the strength of material in this way:

$$stength(z)=\begin{cases} g_1(z)(\sigma_{JC})+\left[1-g_1(z)(\sigma_{JHB})\right], & 0\le z\le h/2 \\ g_2(z)(\sigma_{JC})+\left[1-g_2(z)(\sigma_{JHB})\right], & -h/2\le z\le 0 \end{cases} \tag{19}$$

Where, σ_{JC} and σ_{JHB} are the Johnson-Cook yield stress and JHB failure stress, respectively. The functions, $g_1(z)$, $g_2(z)$, have the same form of equations 17, 18, respectively.

9 CODE VALIDATION

To validate the CSPM code accuracy, a comparison with experimental data [16] has been done in the present work. In this benchmark, the impact of an AL sphere into an AL plate with initial velocity of 6180 m/s has been simulated. The results show good agreements between the numerical results and experimental data.
The values for crater diameter and length/width ratio of the produced debris behind the target for both CSPM and experimental results have been listed in Table 1.

10 NUMERICAL INVESTIGATION

In this section, a general comparison in dynamic behavior of targets with different materials; AL, ALN and AL-ALN FGM has been done under the impact of an AL long rod penetrator. Long rod penetrator impacts normally into the target with initial speed of 10000 m/s. The penetrator includes total number of 600 particles. FGM target was chosen a rectangle with 8mm width and 20mm height with total number of 4000 particles. Total number of 1280 virtual particles was used for wall boundary particles. Figure 2 shows a schematic view of initial configuration of impact simulation. The initial material properties for AL metal and ALN ceramic have been listed in Table 2. The simulation has been done for $5\,\mu s$ after impact. Figure 3 illustrates the yield stress, von-Mises equivalent stress, and velocity distribution for AL target in several time steps during the penetration process. Contours of brittle damage, von-Mises equivalent stress, and velocity distribution for ALN and ALN-AL FGM targets, respectively, have been shown in figures 4 and 5 at several time steps. From the results we can conclude that using the FGM target, a smaller crater diameter in input zone of penetration is produced. The plastic deformation of output zone makes less fragmentation than that in the ALN ceramic target.

In the FGM target, less damage and failure can be seen in comparison with the ALN ceramic target. In the ceramic target, there are larger cracks that propagate near the fixed ends, which there is not such a behavior in the FGM target.

Both ALN and AL-ALN FGM targets has a thinner path of penetration than the AL target.

11 CONCLUSION

In the present paper, a corrective smoothed particle method (CSPM) particle method was implemented to study the dynamic behavior of targets with different materials; AL, ALN and AL-ALN FGM in long rod penetration problem. A combination of Johnson-Cook yield model and JHB failure model using sigmoid function was employed to define the strength model of FGM. Temperature field is evaluated from a heat conduction equation with variable thermal conductivity and the result is used in Johnson-Cook yield model. This study shows that the CSPM method in combination with the proper strength model, can truly handle the plastic and brittle response of different materials in long rod penetration problems.

REFRENCES

[1] Lucy, L.B. A numerical approach to the testing of the fission hypothesis. *Astron. J.* (1977) **82**:1013–1024.

[2] Gingold, R.A. and Monaghan, J.J. Smoothed particle hydrodynamics: theory and application to non-spherical stars. *Mon. Not. R. Astron. Soc*(1977) **181**:375–389.

[3] Monaghan,.J.J. and Kocharyan, A. SPH simulation of multi-phase flow. *Comput. Phys. Commun*(1995) **87**: 225-235.

[4] Monaghan, J.J. Simulating free surface flow with SPH. *J. Comput. Phys*(1994)**110**:399-406.

[5] Morris, J.P. and Fox, P.J. and Zhu, Y. Modeling low Reynolds number incompressible flows using SPH. *J. Comput. Phys*(1997) **136**:214-226.
[6] Antuono, M. and Colagrossi, A. and Marrone, S. and Molteni, D. Free-surface flows solved by means of SPH schemes with numerical diffusive terms. *Comput. Phys. Commun*(2010)**181**:532–549.
[7] Adami, S. and Hu, X.Y. and Adams, N.A. A conservative SPH method for surfactant dynamics. *J. Comput. Phys*(2010) **229**:1909–1926.
[8] Chen, J.K. and Beraun, J.E. and Jih, C.J. An improvement for tensile instability in smoothed particle hydrodynamics. *Comput. Mech*(1999)**23**:279-287.
[9] Tillotson, J.H. Metallic equations of state for hypervelocity impact. *General Dynamics San Diego CA General Atomic Division* (1962)**141**:Report GA-3216.
[10] Johnson, G.R. and Cook, W.H. A constitutive model and data for metals subjected to large strains, high strain rates, and high temperaturas. *Proceeding 7th International Symposium on Ballistics, The Hague, The Netherlands* (1983).
[11] Johnson, G.R. and Holmquist, T.J. and Beissel, S.R. Response of Aluminum Nitride (including a phase change) to large strains, high strain rates, and high pressure. *J. Appl. Phys*(2003) **99:**1639-1646.
[12] Johnson, G.R. and Holmquist, T.J. A computational constitutive model for brittle material subjected to large strains, high strain rates, and high pressures. *14th international symposium on ballistics Quebec, Canada* (1993).
[13] Johnson, G.R. and Holmquist, T.J. An Improved Computational Constitutive Model for Brittle Materials. *High-Pressure Science and Technology, American Institute of Physics* (1993).
[14] Chi, S.H. and Chung, Y.L. Mechanical behavior of functionally graded material plates under transverse load—Part I: Analysis. *Int. J. Solids. Struct* (2006)**43**:3657-3674.
[15] Chi, S.H. and Chung, Y.L. Cracking in sigmoid functionally graded coating. *J. Mech*(2002) **18**: 41–53.
[16] Hiermaier, S. and Konke, D. and Stilp, A.J. and Thoma, K. Computational simulation of the hypervelocity impact of Al-spheres on thin plates of different materials. *Int. J. Impact. Eng*(1997)**20**:363-374.

Table 1: Values for crater diameter and length/width ratio of the produced debris behind the target for both CSPM and experimental results

	SPH Results	***Experimental Data***
Crater Diameter	$3.5\,cm$	$3.45\,cm$
Length / Width Ratio of Produced Debris	1.4 cm	$1.39\,cm$

Table 2: Initial material properties for AL metal and ALN ceramic

	AL Material Properties	***ALN Material Properties***
$Density(kg/m^3)$	2710	3226
Shear Modulus(GPa)	27.1	127
Melting Temperature(kelvin)	775	2370
$Thermal\,coductivity(W/mK)$	250	18
$Specific\,Heat(J/Kg°K)$	875	880
A	265	------
B	426	------
C	0.015	------
m	1	------
n	0.34	------
$K_1(GPa)$	------	201
$K_2(GPa)$	------	260
$K_3(GPa)$	------	0
C_{JHB}	------	0.013
$\sigma_{max}(GPa)$	------	5.22
$Tensile\,limit(GPa)$	------	0.45
$\sigma_i(GPa)$	------	4.31
$P_i(GPa)$	------	1.50
$\sigma_f(GPa)$	------	0.1
$\sigma^f{}_{max}(GPa)$	------	0.2
$P_f(GPa)$	------	0.1

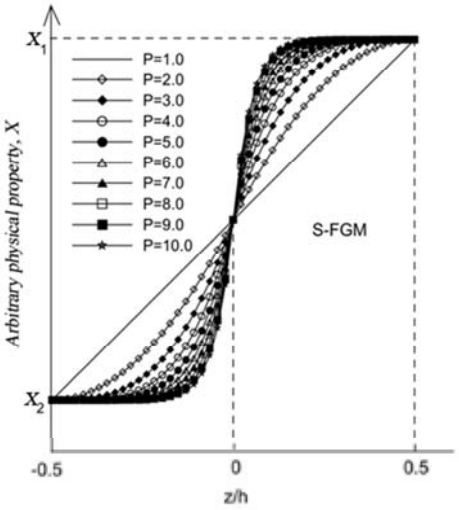

Figure 1: Variation of an arbitrary physical property, X , for different values of P , in a sigmoid FGM plate [14].

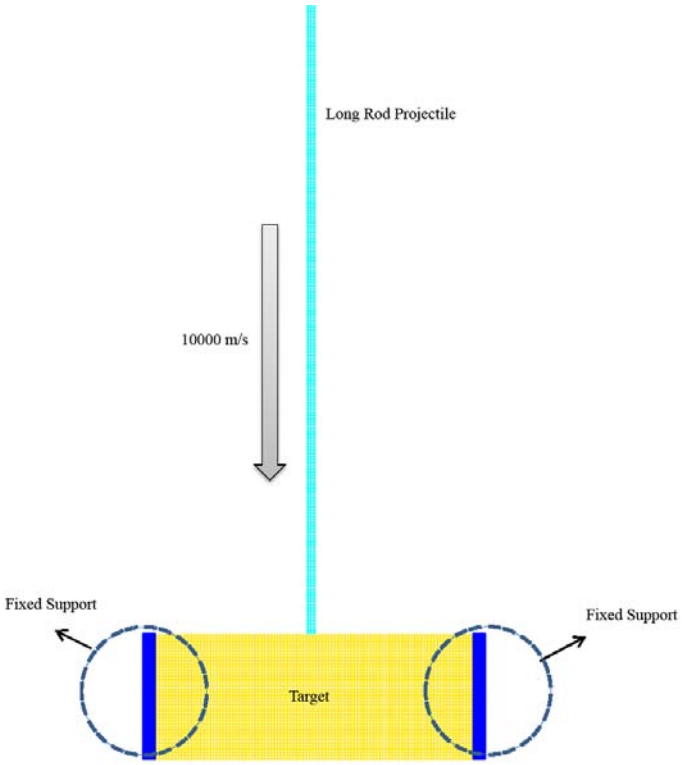

Figure 3: Schematic view of initial configuration of impact simulation

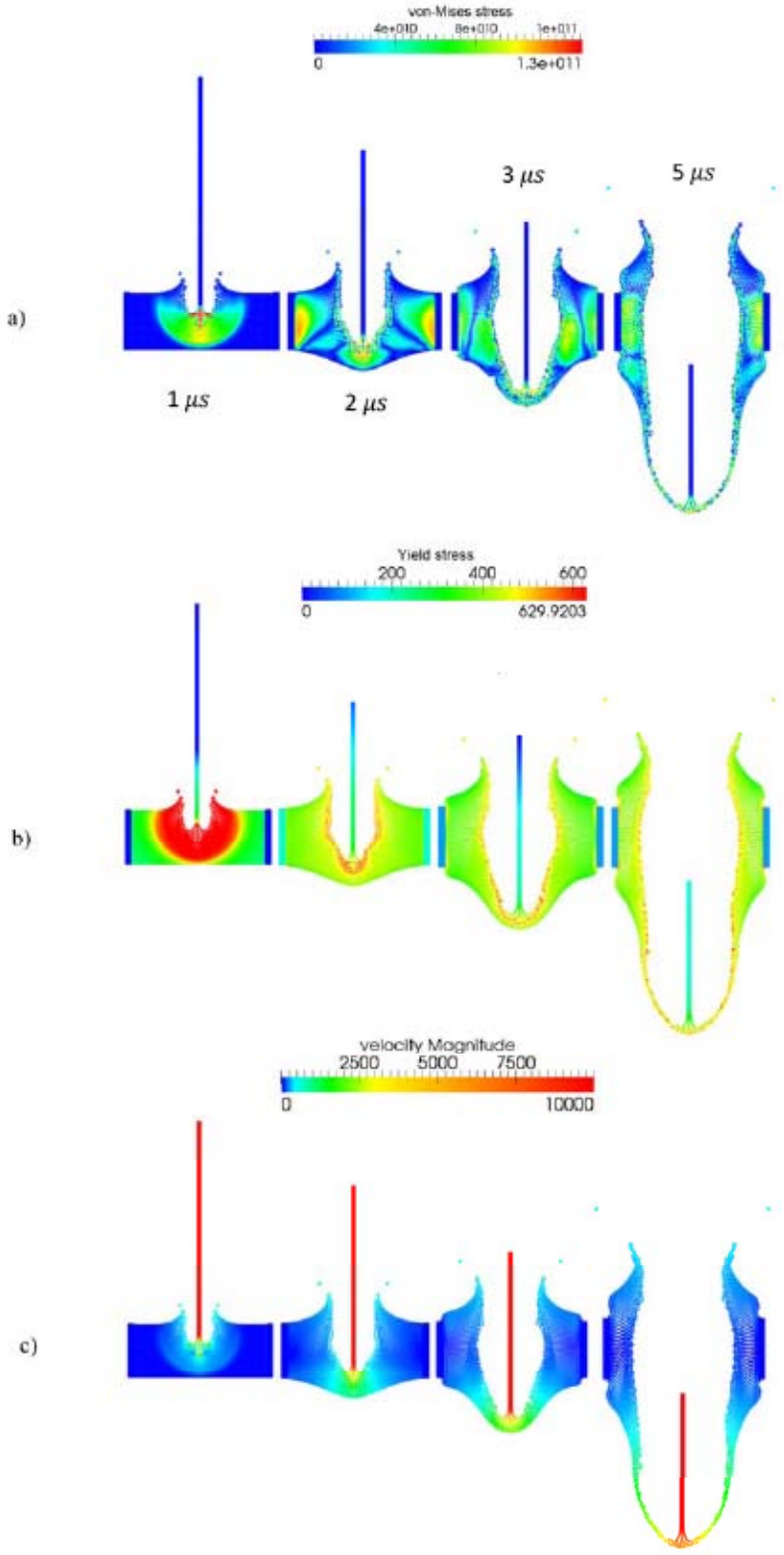

Figure 3: Contour distribution for AL target in several time steps: **a)** von-Mises equivalent stress (Pa), **b)** yield stress (Pa) and **c)** velocity magnitude(m/s)

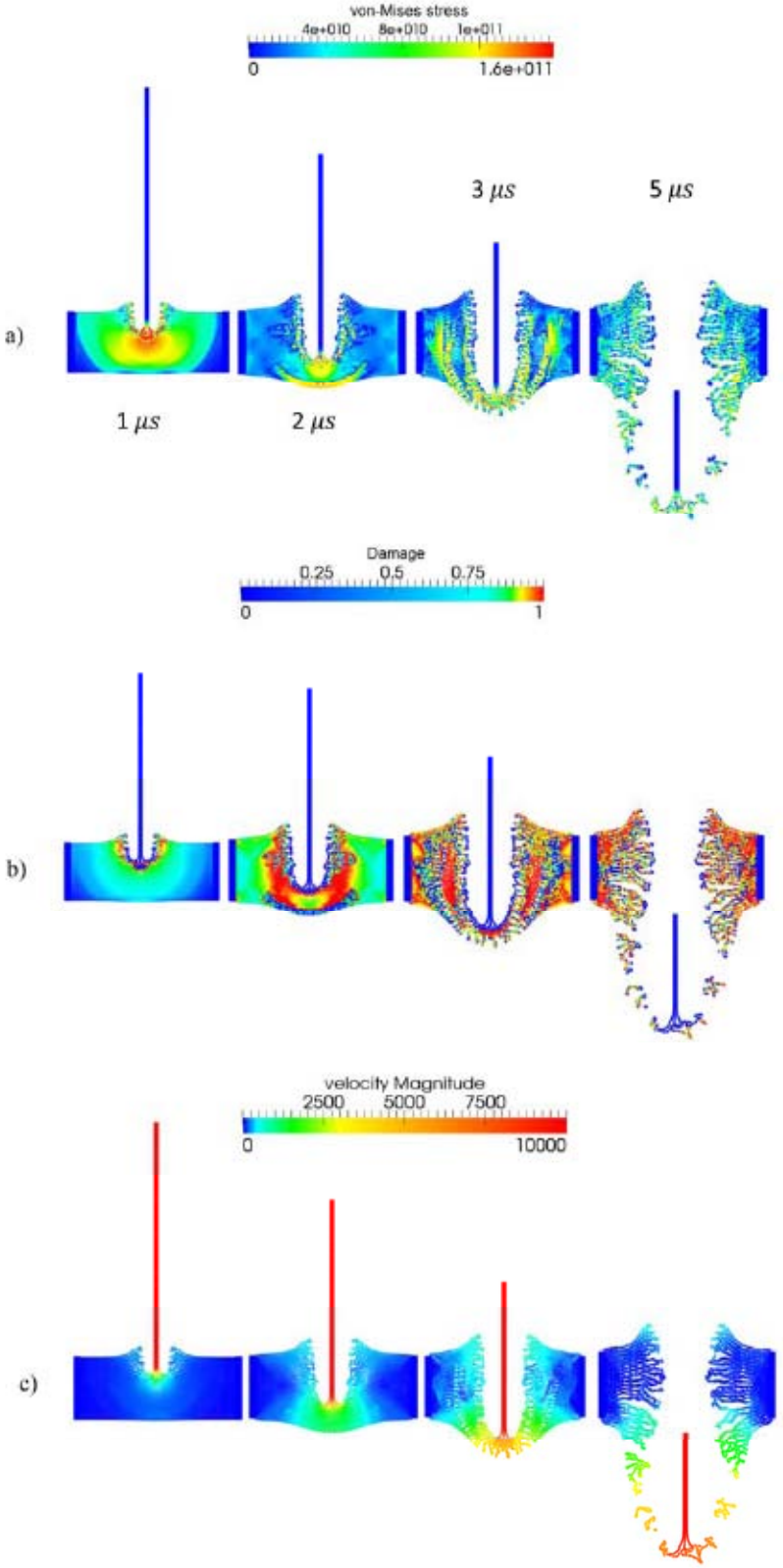

Figure 4: Contour distribution for ALN target in several time steps: **a)** von-Mises equivalent stress (Pa), **b)** Damage and **c)** velocity magnitude (m/s)

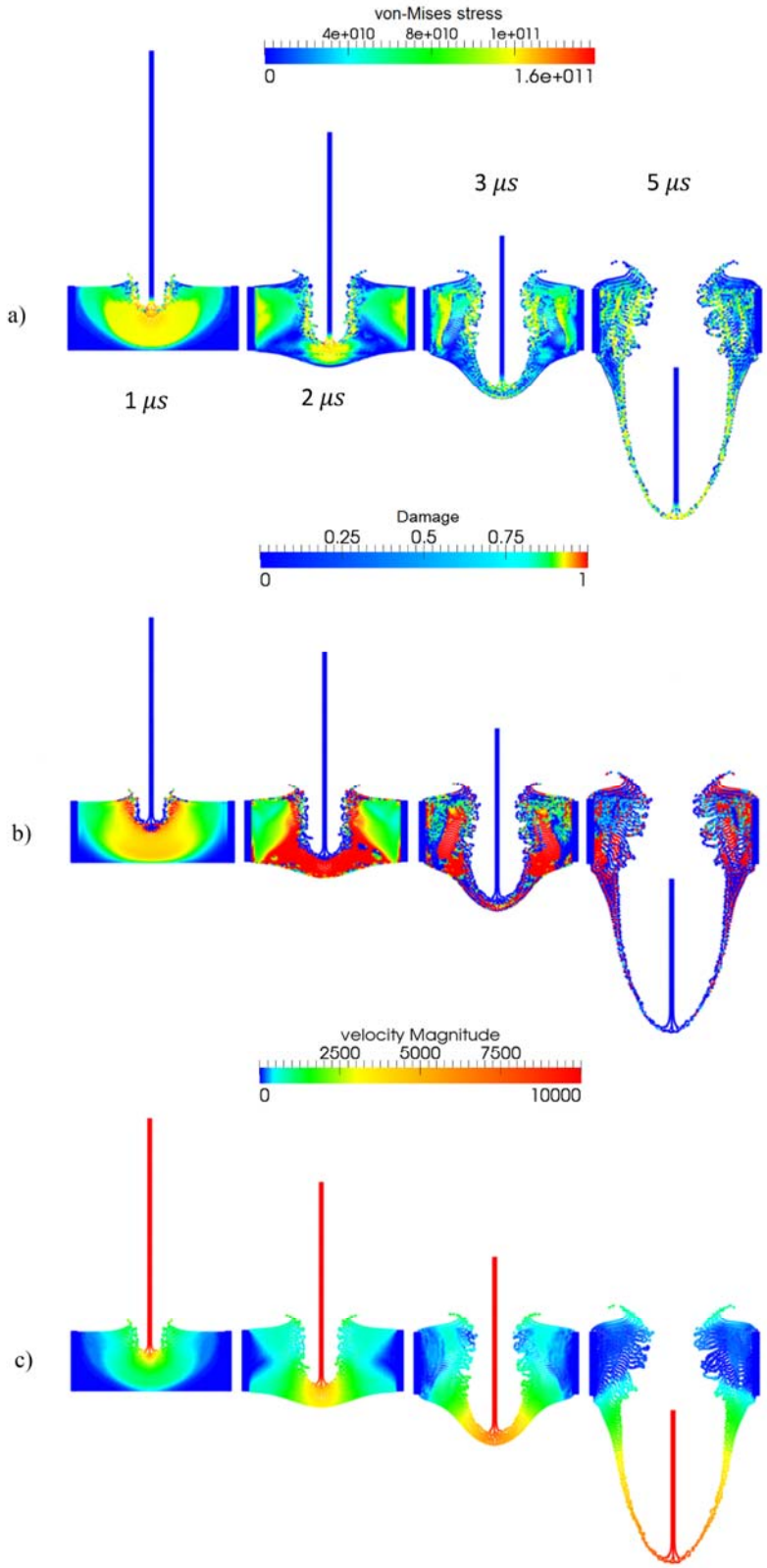

Figure 5: Contour distribution for ALN target in several time steps: **a)** von-Mises equivalent stress (Pa), **b)** Damage and **c)** velocity magnitude (m/s)